Michelson interferometer for precision angle measurement

Masroor Ikram and Ghazanfar Hussain

An angle-measuring technique based on an optical interferometer is reported. The technique exploits a Michelson interferometric configuration in which a right-angle prism and a glass strip are introduced into a probe beam. Simultaneous rotation of both components along an axis results in an optical path difference between the reference and the probe beams. In a second arrangement two right-angle prisms and glass strips are introduced into two beams of a Michelson interferometer. The prisms and the strips are rotated simultaneously to introduce an optical path difference between the two beams. In our arrangement, optimization of various parameters makes the net optical path difference between the two beams approximately linear for a rotation as great as ±20°. Results are simulated that show an improvement of 2–3 orders of magnitude in error and nonlinearity compared with a previously reported technique.

OCIS codes: 120.3180, 120.3940, 220.4830.

1. Introduction

Dynamic angle measurement of an object is an important operation in a number of applications.[1,2] Measurement techniques for small angles (as many as a couple of degrees) have been reported.[3,4] A technique reported by Dai *et al.*[5] is based on reflection of two orthogonal interference patterns from a plane mirror as a rotating object. Their technique is limited to detecting a rotation of as many as 5°. A simple angle-measurement technique that is based on a method of transforming rotation into an optical path difference (OPD) has been reported by Malacara and Harris.[6] In this technique light reflected from the front and the rear surfaces of a plane-parallel glass plate interfere. A change in the OPD between the two beams gives rise to fringe movement that corresponds to the angle of rotation. The technique covers a larger angular range. However, the OPD has a significant nonlinear behavior.

Shi and Stijns[7,8] reported two techniques for rotation sensing that are based on changing the optical path length due to rotation in a Michelson interferometer. In their earlier research, they introduced two right-angle prisms into two arms of the interferometer. Rotation of the prisms along an axis shifts the interference pattern. The technique is very sensitive, but the OPD follows a sinusoidal function of the rotation angle. Later they used one right-angle prism in the probe beam and calculated its optimum position with a parametric compensation method, which improved the linearity in the OPD. We report a technique based on the Michelson interferometer, which reduces the nonlinearity even further for a range of rotation of as many as ±20° and also simplifies the procedure. In our technique we discuss two arrangements. In the first we introduce a single glass strip along with the prism at a certain angle with respect to the input beam, whereas in the second two strips along with two prisms in the interferometer are used to reduce nonlinearity.

2. Principle

In a standard arrangement of the Michelson interferometer, two plane mirrors and a beam splitter form two optical paths. The phase relationship between the two beams is detected in the form of interference fringes at a photodetector. In earlier research[8] a right-angle prism in the probe beam directed the incoming beam toward the end reflecting mirror, M1, as shown in Fig. 1. The diagonal face of the prism was initially perpendicular to the probe beam. When prism P was rotated along an axis $O(0,0)$ the rotation was transformed into the OPD, which was measured

M. Ikram (masroori@yahoo.com) is with the Optics and Laser Group, Pakistan Institute of Engineering and Applied Sciences, P.O. Nilore, Islamabad, Pakistan. G. Hussain is with the Optics Laboratories, P.O. Box 1021, Islamabad, Pakistan.

Received 22 January 1998; revised manuscript received 24 July 1998.

0003-6935/99/010113-08$15.00/0

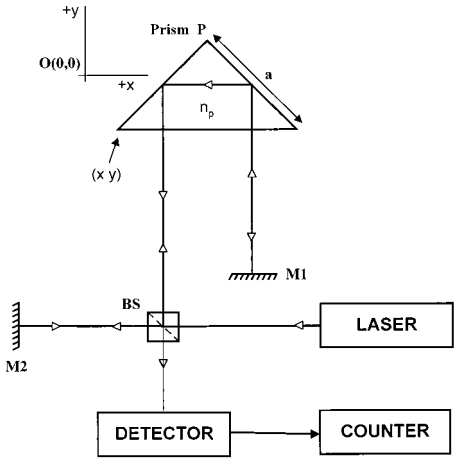

Fig. 1. Michelson interferometer with a right-angle prism P having refractive index n_p in the probe beam. BS, beam splitter; mirrors M1, M2, end reflectors.

by counting the number of fringes across the detector. The optical path length due to rotation of the prism at angle θ is given by[8]

$$\Delta P_O(\theta) = 2x \sin\theta + 2y \tan\left(\frac{\theta}{2}\right)\sin\theta + \sqrt{2}a[(n_p{}^2 - \sin^2\theta)^{1/2} - n_p + \sin\theta], \quad (1)$$

where a, (x, y), and n_p are the side, the vertex coordinates, and the refractive index of the prism, respectively. Equation (1) shows that the change in the OPD is a trigonometric function of the rotation angle. For smaller angles it can be approximated as a linear function. However, it deviates significantly at larger angles.

To reduce this nonlinearity, we introduced a plane transparent glass strip at initial angle ϕ in the probe beam, as shown in Fig. 2. The strip and the prism are placed on the same rotational stage and therefore are rotated simultaneously. The optical path length in the glass strip, which is also a nonlinear function of the rotation angle, is illustrated in Fig. 3. The change in the optical path length due to insertion of the glass strip, at angle ϕ, in the probe beam is given by

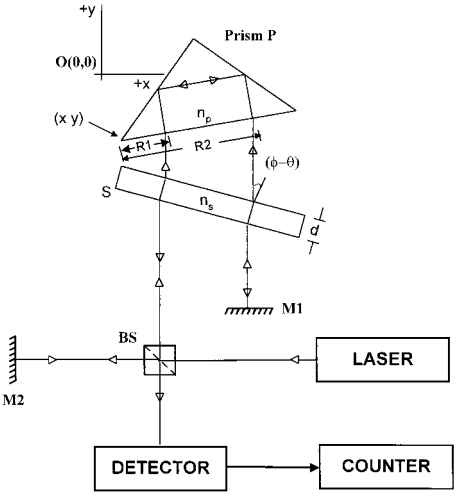

Fig. 2. Michelson interferometer with a plane transparent glass strip S having refractive index n_s of thickness d at an initial angle ϕ with the probe beam. R1, R2, beam intercepts on the diagonal face of the prism.

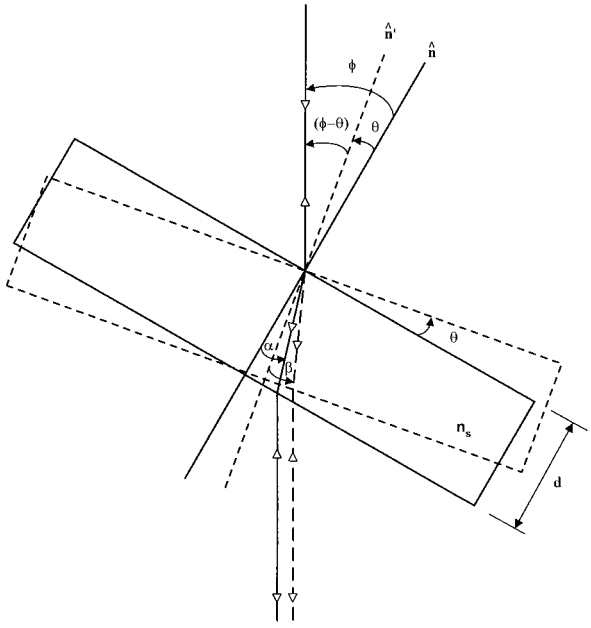

Fig. 3. Optical path of the laser beam through a glass strip of thickness d. Solid lines, initial position of the glass strip at angle ϕ; dashed lines, glass strip after rotation through angle θ; α, β, angles of refraction in the two position.

$$\delta p_S(0) = \frac{n_s d - d\cos(\phi - \alpha)}{\cos\alpha}, \quad (2)$$

where d is the thickness of the glass strip, n_s is the index of refraction, and α is the angle of refraction inside the strip. The change in the optical path length due to rotation of the glass strip through angle θ is given by

$$\delta p_S(\theta) = d\left[\frac{n_s - \cos(\phi - \alpha)}{\cos\alpha} - \frac{n_s - \cos(\phi - \theta - \beta)}{\cos\beta}\right], \quad (3)$$

where β is the angle of refraction when the glass strip is rotated through angle θ from its initial position.

Apart from this change in optical path length there is another source of phase change. According to the Fresnel equations,[9] a phase change takes place upon total internal reflection of light from the two right-angle prism faces. This fact was not taken into account in Eq. (1), which leads to an additional phase

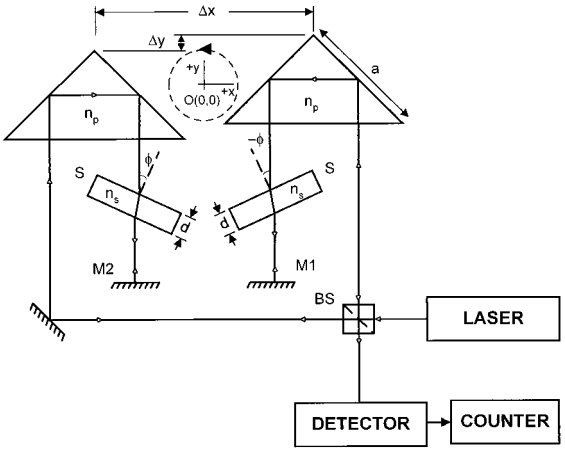

Fig. 4. Michelson interferometer with two prisms and glass strips. Δx, Δy, distances between the apexes of the prisms.

shift Ψ for the total internal reflection of s-polarized light that is given by

$$\Psi = 2\tan^{-1}\left[\frac{(n_p^2\sin^2\{45 - \sin^{-1}[(1/n_p)\sin\theta]\} - 1)^{1/2}}{n_p\cos\{45 - \sin^{-1}[(1/n_p)\sin\theta]\}}\right] - 4\tan^{-1}\left\{\frac{[n_p^2\sin^2(45) - 1]^{1/2}}{n_p\cos(45)}\right\} + 2\tan^{-1}\left[\frac{(n_p^2\sin^2\{45 + \sin^{-1}[(1/n_p)\sin\theta]\} - 1)^{1/2}}{n_p\cos\{45 + \sin^{-1}[(1/n_p)\sin\theta]\}}\right]. \quad (4)$$

Therefore the net OPD after the glass strip is introduced into the probe beam with the prism is expressed as

$$\Delta P_{OS}(\theta) = 2x\sin\theta + 2y\tan\left(\frac{\theta}{2}\right)\sin\theta + \sqrt{2}a[(n_p^2 - \sin^2\theta)^{1/2} - n_p + \sin\theta] + 2d\left[\frac{n_s - \cos(\phi - \alpha)}{\cos\alpha} - \frac{n_s - \cos(\phi - \theta - \beta)}{\cos\beta}\right] + \Psi\frac{\lambda}{360}. \quad (5)$$

The nonlinearity in Eq. (1) can be compensated adequately in Eq. (5) by optimization of x, y, d, and ϕ. Equation (5) shows that the above setup requires accurate positioning of the prism with respect to rotational axis $O(0,0)$, which is also considered as the origin. To address this limitation we introduced a two-prism setup of the Michelson interferometer, as shown in Fig. 4. As before, the diagonal faces of both prisms are perpendicular to the laser beams at the initial position. The change in the optical path length without the strip in the left-hand arm of the interferometer for positive θ (counterclockwise) is given as

$$\delta p_l(\theta) = 2x_1\sin\theta - 2y_1(\cos\theta - 1) + \Psi\frac{\lambda}{360}, \quad (6)$$

where x_1 and y_1 are position coordinates of the prism apex with reference to axis $O(0,0)$. Similarly, the change in the optical path length in the right-hand arm for rotation θ is given by

$$\delta p_r(\theta) = 2x_2\sin\theta - 2y_2(\cos\theta - 1) + \Psi\frac{\lambda}{360}. \quad (7)$$

Therefore the net OPD between the two beams is expressed as

$$\begin{aligned}\Delta P_T(\theta) &= \delta p_r(\theta) - \delta p_l(\theta)\\ &= 2(x_2 - x_1)\sin\theta - 2(y_2 - y_1)(\cos\theta - 1)\\ &= 2\Delta x\sin\theta - 2\Delta y(\cos\theta - 1), \end{aligned} \quad (8)$$

where Δx and Δy are the separations between the two prism apexes in the x and the y directions.

The Fresnel phase, which is introduced simultaneously in the two beams, is mutually canceled at the output. With the glass strips in both arms of the interferometer at initial angle $\pm\phi$, an additional path-length change $\Delta p_{2S}(\theta)$ is introduced and is given by

$$\delta p_{2S}(\theta) = d\left[\frac{n_s - \cos(\phi + \theta + \gamma)}{\cos\gamma} - \frac{n_s - \cos(\phi - \theta - \beta)}{\cos\beta}\right], \quad (9)$$

where β and γ are angles of refraction when glass strips are rotated through angle θ simultaneously with the prism in the left- and the right-hand arms, respectively. Therefore the OPD between the two interfering beams is given by

$$\Delta P_{TS}(\theta) = 2\Delta x\sin\theta + 2\Delta y(\cos\theta - 1) + \delta p_{2S}(\theta). \quad (10)$$

In Eq. (10) optimization of Δx, Δy, d, and ϕ leads to an approximately linear behavior of $\Delta P_{TS}(\theta)$. Equation (10) illustrates that the position of the rotation axis is not critical, and only the distance between prism apexes in the x and the y directions is required.

3. Calculation of Error and Nonlinearity

Ideally it is required that the OPD between the interfering beams $\Delta P(\theta)$ should follow a straight line. The functions expressed by Eqs. (1), (5), and (10) are not perfectly linear. Therefore small deviations in the straight line, which are called errors, can be expressed in terms of the number of fringes,[8] i.e.,

$$\delta(\theta) = (2/\lambda)\Delta P(\theta) - m\theta, \quad (11)$$

where $(2/\lambda)\Delta P(\theta)$ and $m\theta$ represent the actual and the ideal number of fringes, respectively. Sensitivity m is equal to the number of fringes per unit angle.

The degree of nonlinearity Ln is defined as the ratio of error to the ideal number of fringes:

$$Ln = \frac{\delta(\theta)}{m\theta}. \tag{12}$$

The error δ is a function of θ, and for the whole set of equations $\delta(i)$ should be a minimum, i.e.,

$$\sum_{i=1}^{\theta} [\delta(i)]^2 = \min \sum_{i=1}^{\theta} \left[\frac{2}{\lambda}\Delta P(i) - mi\right]^2 = \min \sum_{i=1}^{\theta} \frac{4}{\lambda^2}\left[\Delta P(i) - mi\frac{\lambda}{2}\right]^2. \tag{13}$$

$\Delta P(i)$ is a function of x, y, and d. Therefore the expression in brackets in Eq. (13) can be written in the following form:

$$\sum_{i=1}^{\theta} [\delta(i)]^2 = \min \sum_{i=1}^{\theta} \frac{4}{\lambda^2}(A_i x + B_i y + C_i d + D_i)^2, \tag{14}$$

where A_i, B_i, and C_i are coefficients of x, y, and d. D_i is a constant term. These coefficients have different values in the two cases. For minimizing the error, partial derivatives with respect to x, y, and d of Eq. (13) are to be zero, i.e.,

$$\frac{\partial}{\partial x}\sum_{i=1}^{\theta} [\delta(i)]^2 = 0. \tag{15}$$

Similarly, partial derivatives with respect to y and d can be taken. Substituting the values of $\delta(i)$ from Eq. (14), we get

$$\frac{\partial}{\partial x}\sum_{i=1}^{\theta} (A_i x + B_i y + C_i d + D_i)^2 = 0. \tag{16}$$

Similarly, substitution of the values in other (component) equations will lead to three simultaneous linear equations:

$$x\sum_{i=1}^{\theta}(A_i)^2 + y\sum_{i=1}^{\theta}A_iB_i + d\sum_{i=1}^{\theta}A_iC_i + \sum_{i=1}^{\theta}A_iD_i = 0, \tag{17a}$$

$$x\sum_{i=1}^{\theta}A_iB_i + y\sum_{i=1}^{\theta}(B_i)^2 + d\sum_{i=1}^{\theta}B_iC_i + \sum_{i=1}^{\theta}B_iD_i = 0, \tag{17b}$$

$$x\sum_{i=1}^{\theta}A_iC_i + y\sum_{i=1}^{\theta}C_iB_i + d\sum_{i=1}^{\theta}(C_i)^2 + \sum_{i=1}^{\theta}C_iD_i = 0. \tag{17c}$$

Solution of these equations is expressed in abbreviated form as

$$x = \frac{x_a}{\text{den}}, \tag{18a}$$

$$y = \frac{y_a}{\text{den}}, \tag{18b}$$

$$d = \frac{d_a}{\text{den}}, \tag{18c}$$

where x_a, y_a, d_a, and den (for denominator) are

$$\begin{aligned} x_a = {} & \sum_{i=1}^{\theta}A_iB_i\sum_{i=1}^{\theta}B_iC_i\sum_{i=1}^{\theta}C_i\,D_i \\ & + \sum_{i=1}^{\theta}A_iC_i\sum_{i=1}^{\theta}B_iC_i\sum_{i=1}^{\theta}B_iD_i \\ & - \sum_{i=1}^{\theta}A_iC_i\sum_{i=1}^{\theta}C_iD_i\sum_{i=1}^{\theta}(B_i)^2 \\ & + \sum_{i=1}^{\theta}A_iD_i\sum_{i=1}^{\theta}(B_i)^2\sum_{i=1}^{\theta}(C_i)^2 \\ & - \sum_{i=1}^{\theta}A_iB_i\sum_{i=1}^{\theta}(C_i)^2\sum_{i=1}^{\theta}B_iD_i \\ & - \sum_{i=1}^{\theta}A_iD_i\left(\sum_{i=1}^{\theta}C_iD_i\right)^2, \end{aligned} \tag{19}$$

$$\begin{aligned} y_a = {} & \sum_{i=1}^{\theta}C_iD_i\sum_{i=1}^{\theta}A_iB_i\sum_{i=1}^{\theta}A_iC_i \\ & + \sum_{i=1}^{\theta}A_iC_i\sum_{i=1}^{\theta}B_iC_i\sum_{i=1}^{\theta}A_iD_i \\ & - \sum_{i=1}^{\theta}B_iC_i\sum_{i=1}^{\theta}C_iD_i\sum_{i=1}^{\theta}(A_i)^2 \\ & + \sum_{i=1}^{\theta}B_iD_i\sum_{i=1}^{\theta}(A_i)^2\sum_{i=1}^{\theta}(C_i)^2 \\ & - \sum_{i=1}^{\theta}A_iD_i\sum_{i=1}^{\theta}(C_i)^2\sum_{i=1}^{\theta}A_iB_i \\ & - \sum_{i=1}^{\theta}B_iD_i\left(\sum_{i=1}^{\theta}A_iC_i\right)^2, \end{aligned} \tag{20}$$

$$\begin{aligned} d_a = {} & \sum_{i=1}^{\theta}A_iC_i\sum_{i=1}^{\theta}A_iB_i\sum_{i=1}^{\theta}B_iD_i \\ & + \sum_{i=1}^{\theta}A_iD_i\sum_{i=1}^{\theta}B_iC_i\sum_{i=1}^{\theta}A_iB_i \\ & - \sum_{i=1}^{\theta}B_iC_i\sum_{i=1}^{\theta}B_iD_i\sum_{i=1}^{\theta}(A_i)^2 \\ & + \sum_{i=1}^{\theta}C_iD_i\sum_{i=1}^{\theta}(B_i)^2\sum_{i=1}^{\theta}(A_i)^2 \\ & - \sum_{i=1}^{\theta}A_iD_i\sum_{i=1}^{\theta}(B_i)^2\sum_{i=1}^{\theta}A_iC_i \\ & - \sum_{i=1}^{\theta}C_iD_i\left(\sum_{i=1}^{\theta}A_iB_i\right)^2, \end{aligned} \tag{21}$$

$$\begin{aligned} \text{den} = {} & \sum_{i=1}^{\theta}(A_i)^2\left(\sum_{i=1}^{\theta}B_iC_i\right)^2 \\ & + \sum_{i=1}^{\theta}(C_i)^2\left(\sum_{i=1}^{\theta}A_iB_i\right)^2 \\ & - \sum_{i=1}^{\theta}(A_i)^2\sum_{i=1}^{\theta}(C_i)^2\sum_{i=1}^{\theta}(B_i)^2 \end{aligned}$$

$$+\left(\sum_{i=1}^{\theta} A_i C_i\right)^2 \sum_{i=1}^{\theta} (B_i)^2 - 2\sum_{i=1}^{\theta} A_i C_i \sum_{i=1}^{\theta} A_i B_i \sum_{i=1}^{\theta} B_i C_i. \quad (22)$$

In subsequent discussions these optimized parameters are used to calculate error and nonlinearity in different cases. Optimized parameters x and y in Eqs. (18a) and (18b) represent the coordinates of the left vertex of the prism in the one-prism case, whereas in the two-prism case these parameters represent separation Δx and Δy between the prism apexes.

A. Case i: One Prism with a Glass Strip

The Michelson interferometer with a single prism and a glass strip is shown in Fig. 2. In this setup the OPD between the probe and the reference beams is expressed by Eq. (5), and error $\delta(\theta)$ is obtained by substitution of the OPD in Eq. (11) as

$$\delta(\theta) = \left\{2x \sin\theta + 2y \tan\left(\frac{\theta}{2}\right)\sin\theta + \sqrt{2}a[(n_p{}^2 - \sin^2\theta)^{1/2} - n_p + \sin\theta]\right\}\frac{2}{\lambda} + d\left[\frac{n_s - \cos(\phi - \alpha)}{\cos\alpha} - \frac{n_s - \cos(\phi - \theta - \beta)}{\cos\beta}\right]\frac{4}{\lambda} - m\theta + \frac{\Psi}{180}. \quad (23)$$

Coefficients A_i, B_i, C_i, and D_i of Eq. (14) will be as follows:

$$A_i = 2\sin(i), \quad (24a)$$

$$B_i = 2\tan\left(\frac{i}{2}\right)\sin(i), \quad (24b)$$

$$C_i = \frac{n_s - \cos(\phi - \alpha)}{\cos\alpha} - \frac{n_s - \cos(\phi - i - \beta)}{\beta}, \quad (24c)$$

$$D_i = \sqrt{2}a\{[n_p{}^2 - \sin^2(i)]^{1/2} - n_p + \sin(i)\} - mi\frac{\lambda}{2} + \Psi\frac{\lambda}{360}. \quad (24d)$$

B. Case ii: Two Prisms with Glass Strips

For a Michelson interferometer with two prisms and glass strips, the OPD between two interfering beams is expressed by Eq. (10). The error $\delta(\theta)$ in this case is given by

$$\delta(\theta) = [2\Delta x \sin\theta + 2\Delta y(\cos\theta - 1)]\frac{2}{\lambda} - m\theta + \frac{2d}{\lambda}\left[\frac{n_s - \cos(\phi + \theta + \gamma)}{\cos\gamma} - \frac{n_s - \cos(\phi - \theta - \beta)}{\cos\beta}\right]. \quad (25)$$

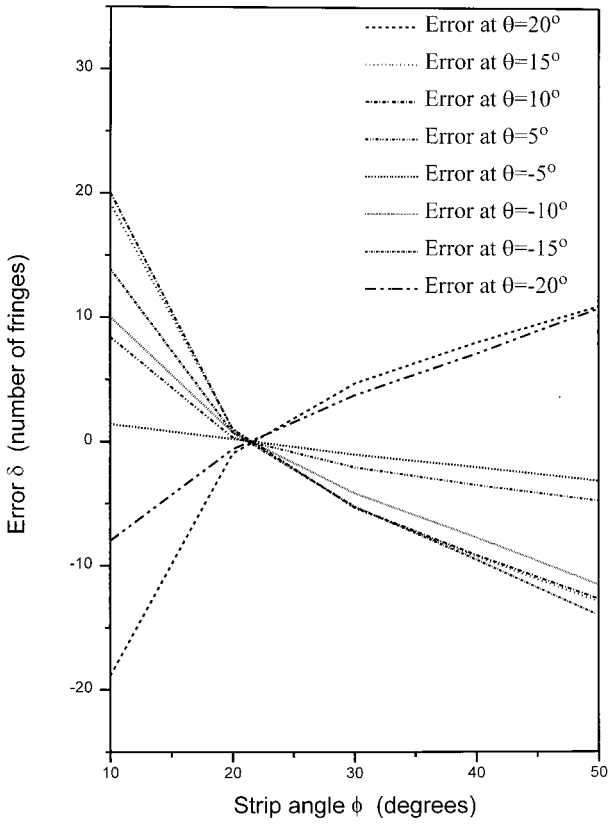

Fig. 5. Plot of error function [Eq. (23)] against initial angle ϕ of the glass strip to as great as $\pm 20°$.

Coefficients A_i, B_i, C_i, and D_i of Eq. (14) in this case are

$$A_i = 2\sin(i), \quad (26a)$$

$$B_i = 2[\cos(i) - 1], \quad (26b)$$

$$C_i = \frac{n_s - \cos(\phi + i + \gamma)}{\cos\gamma} - \frac{n_s - \cos(\phi - i - \beta)}{\cos\beta}, \quad (26c)$$

$$D_i = mi\frac{\lambda}{2}. \quad (26d)$$

The error and the nonlinearity defined in Eqs. (11) and (12) are calculated for the two cases.

4. Results and Discussion

Angle measurement with interferometric techniques suffers from nonlinearity in the OPD. Shi and Stijns[8] have reduced the nonlinearity in the OPD by using a parametric compensation method. For a rotation range of $\pm 5°$ the maximum error in their technique is nearly 18 fringes. However, we have reduced the error and nonlinearity by optimization of prism positions, the thickness of glass strips, and their angles. The error and the nonlinearity in our technique are simulated for larger angular ranges.

Figure 5 shows a plot of Eq. (23) for minimum error. In the first step, the value of $+\theta$ is kept fixed while we varied ϕ in steps from 10° to 50° to calculate

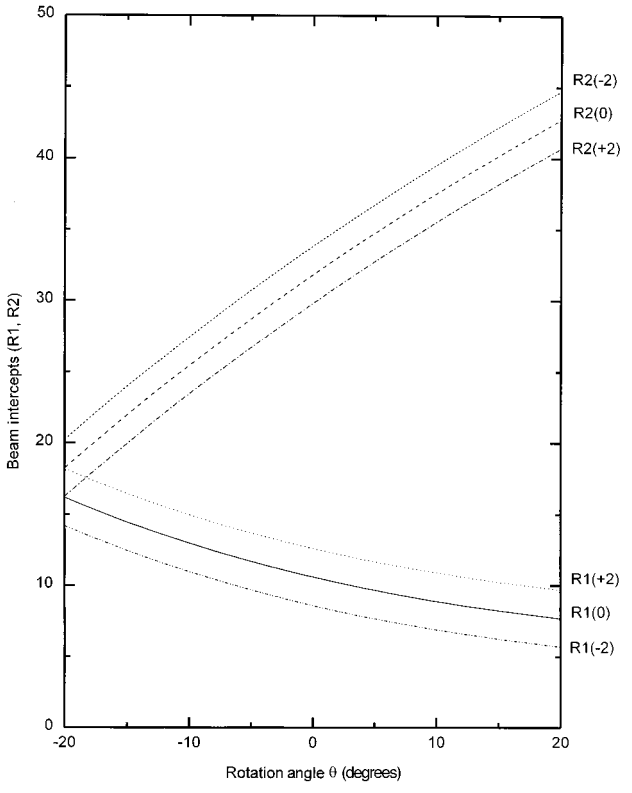

Fig. 6. Plot of beam intercepts R1 and R2 for the one-prism case.

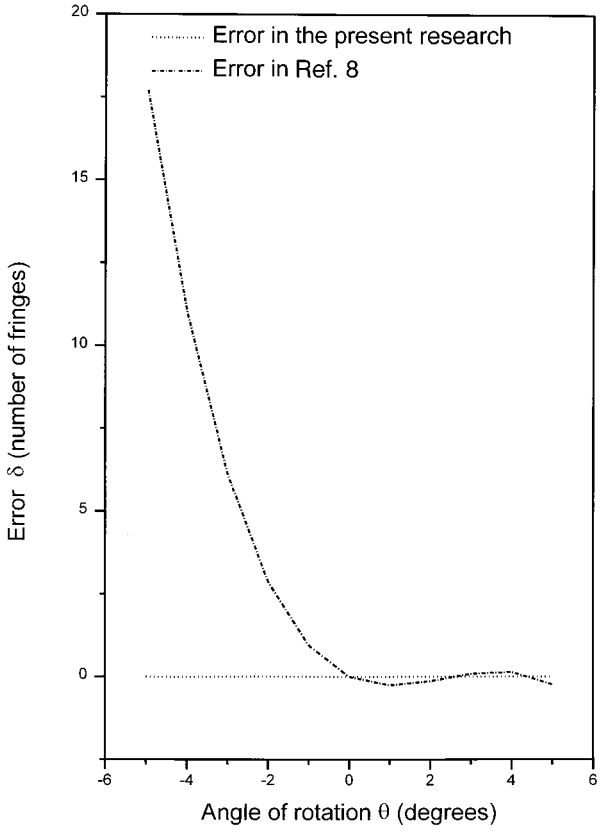

Fig. 7. Comparison of error in the present research with the research of Shi and Stijns[8] for a rotation range of ±5°.

coefficients A, B, C, and constant D. In the second step the values of these coefficients are substituted into Eqs. (18) to achieve the optimized values of x, y, and d. Subsequently we substituted a set of these values into Eq. (23) to draw a curve for the fixed value of $+\theta$. We repeated these steps to draw a curve for $-\theta$. The intersection point between the pair of curves for $\pm\theta$ gives the common minimum error at strip angle ϕ. The intersection points for the pairs of curves change in a complex manner. All these points tend to converge within a close region. Twenty such curves are drawn to achieve the optimized value of ϕ. However, only eight of these curves are shown in Fig. 5. We have selected the midpoint along the y axis between the extreme intersection points and taken its corresponding strip angle as the optimized one. The optimized values of ϕ for ranges of rotation as great as ±5°, ±10°, and ±20° are 26.8°, 21.3°, and 21.15°, respectively. Similarly, in the two-prism case the optimum values of ϕ for rotation ranges of ±10° and ±20° are 38.55° and 37.1°, respectively.

Figure 6 shows the behavior of the incident and the exit probe beams in the one-prism case at the optimized parameters for the range of ±20°. Beam intercepts R1 and R2 are the distances of the incident and the exit beams from the left-hand-side vertex (x, y) of the prism. As the intercept of the incident beam decreases, the exit beam moves farther from the vertex. Curves R1(0) and R2(0) show the beam intercepts when the incident and the exit beams enter the prism initially (at $\theta = 0$) at distances of 10.60 and 31.81 mm from the vertex, respectively. As the value of $+\theta$ increases, intercepts of the incident beam decrease while they increase for the exit beam. At +20° the exit beam just emerges from the prism without reflection from the second face. For rotation angle $-\theta$ this beam has the reverse trend. Curves R1(+2) and R1(−2) show that incident-beam intercepts are shifted from their initial intercept values to 10.6 ± 2 mm, respectively, while R2(+2) and R2(−2) are the corresponding exit-beam intercepts.

Figure 7 shows a comparison between the one-prism technique of Shi and Stijns[8] and ours for rotation to as great as ±5°. Results are simulated for the initial setting of the prism side, $a = 30$ mm, the refractive index of the prism and glass strip to 1.517, and the sensitivity of 1000 fringes/deg. The optimized parameters are $x = -14.9126$, $y = 20.8463$, and $d = 15.943$. The fringe sign is negative for clockwise rotation. The maximum error in their technique is 17.95 fringes, whereas in our case it is 0.0045 fringes. Similarly, nonlinearity is also reduced, which is 3 orders better and is written with a multiplication factor of 10^{-6}. Therefore the error in the present case is significantly reduced compared with the technique of Shi and Stijns.[8]

Figure 8 shows the results of the one- and the two-prism cases for a rotation range of ±10° with $a = 30$. The parameters for the two cases are as follows: the one-prism case ($x = -15.8723$, $y = 22.1812$, $d =$

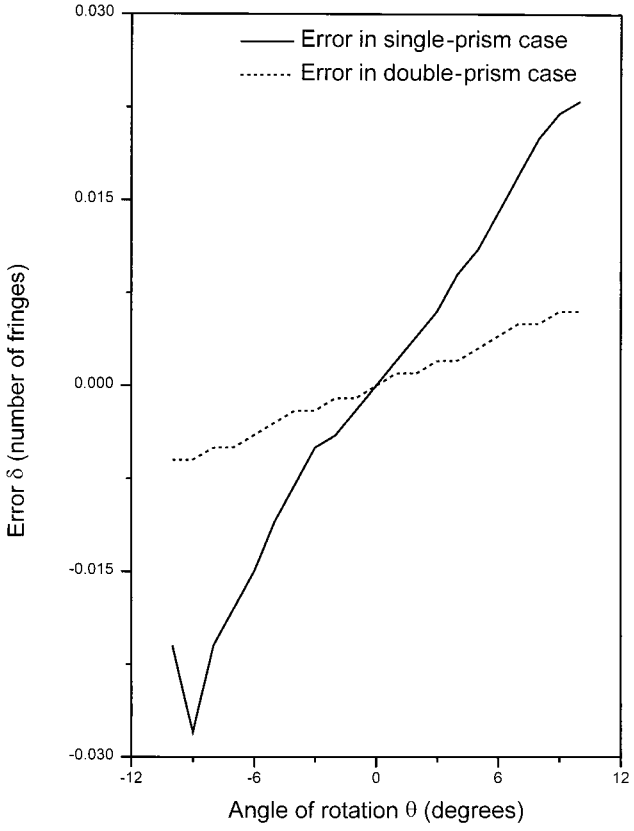

Fig. 8. Error in the single- and the double-prism cases for a rotation range of ±10°.

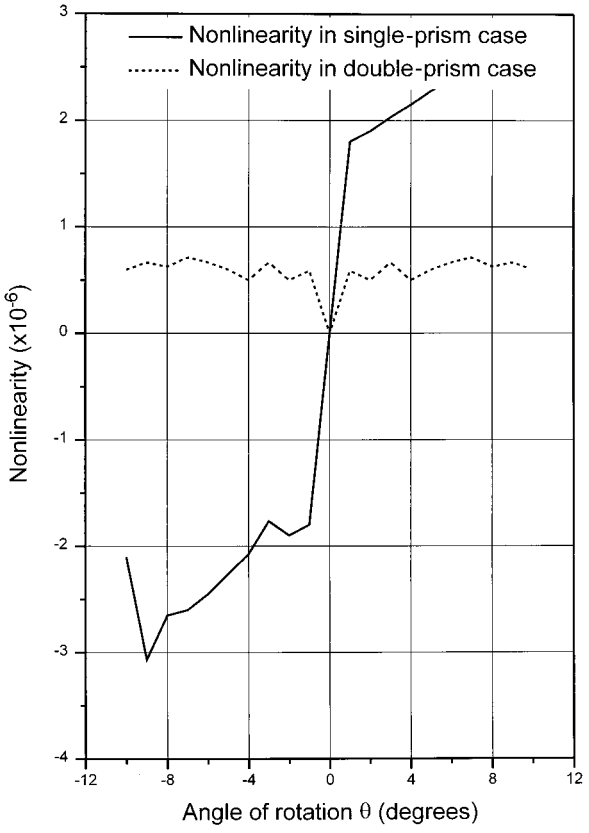

Fig. 9. Nonlinearity present in the single- and the double-prism case for rotation to as great as ±10°.

Table 1. Error and Nonlinearity in One- and Two-Prism Setups for ±20 deg

Angle θ (deg)	Total No. of Fringes N	One Prism[a] Error (No. of Fringes) $\delta = 2\Delta P/\lambda - N$	One Prism[a] Nonlinearity $Ln = \delta/N$ (1/1,000,000)	Two Prism[b] Error (No. of Fringes) $\delta = 2\Delta P/\lambda - N$	Two Prism[b] Nonlinearity $Ln = \delta/N$ (1/1,000,000)
−20	−20000	0.040	−2.015	0.032	−1.600
−18	−18000	−0.043	2.361	0.009	−0.500
−16	−16000	−0.053	3.281	0.011	−0.688
−14	−14000	−0.030	2.157	0.017	−1.214
−12	−12000	0.000	0.038	0.019	−1.583
−10	−10000	0.023	−2.320	0.016	−1.600
−8	−8000	0.035	−4.388	0.010	−1.250
−6	−6000	0.035	−5.883	0.005	−0.833
−4	−4000	0.027	−6.650	0.001	−0.250
−2	−2000	0.023	−11.725	0.000	0.135
0	0	0.000	0.000	0.000	0.000
2	2000	−0.010	−5.050	0.000	0.135
4	4000	−0.015	−3.625	−0.001	−0.250
6	6000	−0.013	−2.117	−0.005	−0.833
8	8000	−0.005	−0.650	−0.010	−1.250
10	10000	0.006	0.550	−0.016	−1.600
12	12000	0.016	1.358	−0.019	−1.583
14	14000	0.023	1.643	−0.017	−1.214
16	16000	0.021	1.300	−0.011	−0.688
18	18000	0.005	0.267	−0.009	−0.500
20	20000	0.030	1.510	−0.032	−1.600

[a] $x = -15.878$ mm, $y = 22.2649$ mm, $d = 42.6596$ mm, $n_p = n_s = 1.84489$ (LaSF N9 of Schott), $\phi = 21.15°$.
[b] $\Delta x = 6.2513$ mm, $\Delta y = 0.0000$ mm, $d = 10.9432$ mm, $n_p = 1.84489$, $n_s = 1.51509$ (BK7 of Schott), $\phi = 37.1°$.

21.138, $\phi = 21.3°$, $n_p = n_s = 1.84489$, LaSF N9 Schott) and the two-prism case ($\Delta x = 6.2342$, $\Delta y = 0.0$, $d = 10.4708$, $\phi = 38.55°$, $n_s = 1.509$, BK7, $n_p = 1.84489$). The main reason for choosing a higher refractive index ($n_p = 1.84489$) is to fulfill the requirements of the total internal reflection from the two-prism faces for rotation ranges of $\pm 10°$ and $\pm 20°$. The maximum error for the one- and the two-prism cases are -0.028 and $+0.006$ fringes, respectively, for rotation as great as $\pm 10°$. Similarly, maximum nonlinearity, as shown in Fig. 9, in both cases is 3.067×10^{-6} and 7.14×10^{-7}, respectively. The overall error and nonlinearity increase for the larger angular ranges in both cases. This increase is due to the inherent nonlinearity in the OPD as expressed in Eqs. (5) and (10). Smaller values of Δx and Δy in the second case limit the two prisms to be placed in the same plane. Therefore in such a situation prisms are to be placed in two parallel planes, i.e., one on top of the other, in the required shifts Δx and Δy.

A similar trend of increase in error and nonlinearity is achieved for a rotation range of $\pm 20°$, as shown in Table 1. Here a comparison between the one- and the two-prism cases shows that the two-prism case performs better and also has other advantages:

(1) Mechanical dimensions of x, y, and d are smaller for the same sensitivity.

(2) The axis of rotation is not restricted to a single point because the equation of the path length specifies Δx and Δy instead of x and y.

(3) The sensitivity of the interferometer can be increased by a corresponding increase in the dimensions of the interferometer.

5. Conclusion

A technique for precision angle measurement has been presented that is based on the Michelson interferometer. We have reported two cases of measurement for rotation ranges of $\pm 5°$, $\pm 10°$, and $\pm 20°$. Optimization of the position of the prisms, the thickness of the glass strips, and their angle contributes to improvement in the linearity of the OPD. Results have been compared with a previously reported technique to show a reduction in error of more than 3 orders of magnitudes. The two-prism case has shown better linearity and less error compared with the one-prism case, especially for longer angular ranges. However, the overall error and the nonlinearity are increased for longer ranges. The two-prism case does not require any particular position for the rotation axis. The interferometer has good accuracy and can be used for micrometrological applications, in spectrometers, for rotational stages, for rotational seismic pickups, for calibration of robots, etc.

References

1. M. Ben-Levy, S. G. Braun, and J. Shamir, "Angular velocity measuring interferometer," Appl. Opt. **18,** 4265–4266 (1989).
2. H. K. Chiang, R. P. Kenan, N. F. Hartman, and C. J. Summers, "Optical alignment and tilt angle measurement technique based on Lloyd's mirror arrangement," Opt. Lett. **17,** 1024–1025 (1992).
3. L. Zeng, H. Mataumoto, and K. Kawachi, "Scanning beam collimation method for measuring dynamic angle variations using an acousto-optic deflector," Opt. Eng. **35,** 1662–1667 (1996).
4. I. Shavirin, O. Strelkov, A. Vetskous, L. Norton-Wayne, and R. Harwood, "Internal reflection sensors with high angular resolution," Appl. Opt. **35,** 4133–4141 (1996).
5. X. Dai, O. Sasaki, J. E. Greivenkamp, and T. Suzuki, "Measurement of two-dimensional small rotation angles by using orthogonal parallel interference patterns," Appl. Opt. **35,** 5657–5666 (1996).
6. D. Malacara and O. Harris, "Interferometric measurement of angles," Appl. Opt. **9,** 1630–1633 (1970).
7. P. Shi and E. Stijns, "New optical method for measuring small-angle rotations," Appl. Opt. **27,** 4342–4344 (1988).
8. P. Shi and E. Stijns, "Improving the linearity of the Michelson interferometric angular measurement by a parametric compensation method," Appl. Opt. **32,** 44–51 (1993).
9. F. A. Jenkins and H. E. White, *Fundamentals of Optics*, 4th ed. (McGraw-Hill, Singapore, 1985), p. 529.